Ultrasensitive hysteretic force sensing with parametric nonlinear oscillators

Luca Papariello, Oded Zilberberg, Alexander Eichler, and R. Chitra

Department of Physics, ETH Zurich, 8093 Zürich, Switzerland

We propose a method for linear detection of weak forces using parametrically driven nonlinear resonators. The method is based on a peculiar feature in the response of the resonator to a near resonant periodic external force. This feature stems from a complex interplay among the parametric drive, external force, and nonlinearities. For weak parametric drive, the response exhibits the standard Duffing-like single jump hysteresis. For stronger drive amplitudes, we find a qualitatively new double jump hysteresis which arises from stable solutions generated by the cubic Duffing nonlinearity. The additional jump exists only if the external force is present and the frequency at which it occurs depends linearly on the amplitude of the external force, permitting a straightforward ultrasensitive detection of weak forces. With state-of-the-art nanomechanical resonators, our scheme should permit force detection in the attonewton range.

I. INTRODUCTION

Research on nonlinear resonators started over a century ago, motivated by observations in electrodynamics and mechanics [1]. The fact that novel features are still discovered in nonlinear resonators today bears witness to their great complexity and variety. Nonlinear resonators manifest themselves in many modern fields of physics, e.g., quantum electrical circuits, cold atoms, levitated nanoparticles, and nanoelectromechanical systems (NEMS) [2]. They are intimately related to state-of-the-art metrology platforms used for measurements of weak external forces corresponding to single charges, spins, or mass on the atomic scale [3–6].

Interestingly, many of these modern resonators allow the study of individual modes whose nonlinearities can be tailored or tuned *in situ* and on which theoretical concepts, both classical and quantum, can be tested [7,8]. One such concept is parametric resonance, where the frequency of the linear oscillator is modulated in time [9]. The parametrically driven oscillator boasts a fascinating stability diagram called "Arnold's tongues" delineating zones where the oscillator is stable from those where it is exponentially unstable as a function of its natural frequency and parametric driving strength [10]. In the stable regime, parametric resonance can be used to amplify signals and squeeze noise [9,11,12], design mechanical logic circuits [13], or generate quantum entanglement [14,15]. In the unstable regime, the resonator is driven to a large and stable response, which can be used for mechanical information storage [16] or signal amplification through bifurcation topology [17].

Nonlinearities become important as resonators scale down [18]. This can be attributed to geometric effects, external potentials, dissipation, or even feedback cooling used to control the resonator. Nonlinear effects strongly restrict the dynamic range within which the system operates linearly, even making it vanishingly small in NEMS, and limit the scope for applications. However, recent works focus on directly using nonlinearities to improve the sensitivity of parametrically amplified detectors [17,19,20]. For instance, though quartic (Duffing) nonlinearities stabilize the parametric oscillator, it retains a "memory" of the underlying instability tongue structure in its frequency dependent response [21]. The

precision measurement of this lobe [19,21] then provides a very robust and stable way of detecting masses [19]. Still, the utility of nonlinearities in parametrically driven oscillators for sensing of external forces remains relatively unexplored.

In this work we obtain a solution for the response of an externally driven nonlinear parametric resonator below and beyond the instability threshold. The response features an unexpected double hysteresis whose position depends sensitively and linearly on the amplitude of the applied external force. Using recent experiments as examples, we predict how the double hysteresis should manifest, and we propose a method to use it for the detection of weak forces. Importantly, the force sensor we propose has a linear dependency of signal on measured force even though it is based on a nonlinear mechanical resonator.

The article is structured as follows. In Sec. II, we detail the model describing a general nonlinear parametric oscillator model. Section III is dedicated to a short description of the perturbative averaging method used for the analysis of the model used to obtain a closed equation for the steady-state positional response. Based on our results for the response, we present our method for hysteretic force detection in Sec. IV. In the concluding section, we discuss the application of our force detection scheme to different experimental systems. Discussion of the limiting cases and known results are relegated to the Appendices.

II. MODEL

The equation of motion governing the dynamics of a parametrically driven nonlinear oscillator of mass m subject to a periodic external force is

$$m\ddot{x} + m\omega_0^2(1 - \lambda \cos \omega_p t)x + \gamma \dot{x} + \alpha x^3 + \eta x^2 \dot{x}$$
$$= F_0 \cos \omega_f t, \tag{1}$$

where ω_0 is the unperturbed frequency of the linear oscillator, γ is the linear damping, and λ and ω_p denote the strength and frequency of the parametric drive. Parametric resonance occurs whenever the parametric drive frequency satisfies the condition $\omega_p = 2\omega_0/n$, where n is an integer which labels the instability zones. The effects of parametric driving are most

pronounced for $n \sim 1$. The nonlinearities are described by the Duffing parameter α characterizing the quartic contribution to the oscillator potential, and η denotes the strength of the nonlinear feedback cooling or nonlinear damping that is present in generic experimental setups [22,23]. Though nonlinearities stabilize the regions of instability [1,21], the nonlinear parametric resonator retains a precise memory of the instability regions of the parametric linear oscillator (see Appendix B).

The term on the right-hand side of (1) refers to a periodic external force of strength F_0 and frequency ω_f. Equation (1) generically describes the physics of resonators realized in a wide range of experimental setups. Though a vast literature exists on the solutions to this equation in various regimes [1,24], surprisingly, the impact of a periodically modulated external force on the full nonlinear problem has not been studied in great detail. In the following we consider a positive Duffing parameter α. Our methodology and results can be straightforwardly extended to the case of negative Duffing coefficients (as will be discussed later).

The main focus of this work involves studying the response of a parametric resonator to an external force, $F_0 \neq 0$, in the nonlinear regime. Bifurcations arise in this problem which essentially change the nature of the associated response. Equation (1) is a nonautonomous, inhomogeneous, and nonlinear differential equation that does not permit an analytic solution for generic parameters. In typical experiments, the focus is on the first parametric resonance of the system, i.e., operating around twice the bare frequency of the undriven oscillator $\omega_p \approx 2\omega_0$ while the frequency of the external drive is $\omega_f \approx \omega_0$. As we will show, approximate analytic solutions to the frequency-dependent response can be obtained in these experimentally relevant parameter regimes.

III. RESPONSE FUNCTION

To analyze the equation of motion [Eq. (1)] we use the perturbative averaging method [25], which replaces the full time-dependent equation by time-independent averaged equations of motion. Before that, we redefine time and space in Eq. (1) according to $\tau = \omega_0 t$ and $z = x\sqrt{\alpha/m\omega_0^2}$. This leads to the dimensionless equation of motion,

$$\ddot{z} + \bar{\gamma}\dot{z} + z^3 + \bar{\eta}z^2\dot{z} + (1 - \lambda\cos 2\Omega\tau)z = \bar{F}_0\cos(\Omega\tau + \vartheta), \tag{2}$$

where the dimensionless parameters are defined as $\bar{\gamma} \equiv \gamma/m\omega_0 = 1/Q$, $\bar{\eta} \equiv \eta\omega_0/\alpha$, $\Omega \equiv \omega/\omega_0$, and $\bar{F}_0 \equiv (F_0/\omega_0^3)\sqrt{\alpha/m^3}$. Using this method, the frequency region around the first instability lobe is parametrized by setting $\omega_p = 2\omega$, with $\omega \approx \omega_0$. Additionally, we introduce a detuning parameter $\sigma = 1 - \Omega^2$. Furthermore, the frequency of the external drive is locked at half the value of the parametric pump frequency $\omega_f = \omega$, with a relative phase ϑ between the two drives. With the parameters so defined, Eq. (1) can be recast as a pair of first-order equations

$$y = \dot{z}, \tag{3}$$

$$\dot{y} + \Omega^2 z = f(z,y,\tau), \tag{4}$$

with

$$f(z,y,\tau) = -\sigma z - \bar{\gamma}y - z^3 - \bar{\eta}z^2 y + \lambda\cos(2\Omega\tau)z + \bar{F}_0\cos(\Omega\tau + \vartheta), \tag{5}$$

Note that in order for the present perturbative method to be valid, the detuning σ, linear and nonlinear damping $\bar{\gamma}$ and $\bar{\eta}$, as well as the driving strengths λ and $\bar{F}_0$ have to be small. Since Eqs. (3)–(5) are dimensionless, the true range of forces that can be studied with this perturbative method depends on the particular realization of the nonlinear resonator. The next step consists in bringing Eq. (4) into the so-called standard form for averaging, i.e., into a form $\dot{z} = \epsilon f(z,y,\tau)$ with $0 < \epsilon \ll 1$. This is accomplished using the van der Pol transformation [25] to variables U and V,

$$\begin{bmatrix} z \\ y \end{bmatrix} = \begin{bmatrix} \cos\Omega\tau & -\sin\Omega\tau \\ -\Omega\sin\Omega\tau & -\Omega\cos\Omega\tau \end{bmatrix} \begin{bmatrix} U \\ V \end{bmatrix}. \tag{6}$$

Substituting (6) into (4) and averaging over the time period $T = 2\pi/\Omega$, we obtain the equations for the slow flow variables $u = \overline{U}$ and $v = \overline{V}$, which correspond to time-averaged U and V over the time cycle:

$$\dot{u} = -\frac{1}{2\Omega}\left[\bar{\gamma}\Omega u + v\left(\sigma + \frac{\lambda}{2}\right) + \frac{3}{4}(u^2 + v^2)v + \Omega\frac{\bar{\eta}}{4}(u^2 + v^2)u - \bar{F}_0\sin\vartheta\right], \tag{7}$$

$$\dot{v} = -\frac{1}{2\Omega}\left[\bar{\gamma}\Omega v + u\left(-\sigma + \frac{\lambda}{2}\right) - \frac{3}{4}(u^2 + v^2)u + \Omega\frac{\bar{\eta}}{4}(u^2 + v^2)v + \bar{F}_0\cos\vartheta\right]. \tag{8}$$

Despite the perturbative nature of the averaging method, it is valid for a surprisingly large range of values of the drive amplitude λ as well as for substantial detuning Ω [26]. However, to access the full range of the system parameters as well as more complex nonlinearities, one would need to do a full numerical study.

The coupled slow flow Eqs. (7) and (8) remain analytically insolvable. However, from the perspective of measurements, one only needs to know the frequency response of the oscillator $|\bar{X}| = (u^2 + v^2)^{1/2}$. This is a property of the steady state and does not require knowledge of transients. Consequently, in the steady state, we set $\dot{u} = \dot{v} = 0$ in Eqs. (7) and (8), and we find that the response $|X|^2$ satisfies the following polynomial equation:

$$|\bar{X}|^2\left[\left(\bar{\gamma}\Omega + \frac{\bar{\eta}}{4}\Omega|\bar{X}|^2\right)^2 - \left(\frac{\lambda}{2}\right)^2 + \left(\sigma + \frac{3}{4}|\bar{X}|^2\right)^2\right]^2$$

$$= \bar{F}_0^2\left[\left(\bar{\gamma}\Omega + \frac{\bar{\eta}}{4}\Omega|\bar{X}|^2\right)^2 + \left(\frac{\lambda}{2}\right)^2 + \left(\sigma + \frac{3}{4}|\bar{X}|^2\right)^2\right.$$

$$\left. + \lambda\left(\sigma + \frac{3}{4}|\bar{X}|^2\right)\cos 2\vartheta + \lambda\left(\bar{\gamma}\Omega + \frac{\bar{\eta}}{4}\Omega|\bar{X}|^2\right)\sin 2\vartheta\right]. \tag{9}$$

Equation (9) determines the response in a finite frequency interval ω around ω_0. Obtaining the response for arbitrary ω
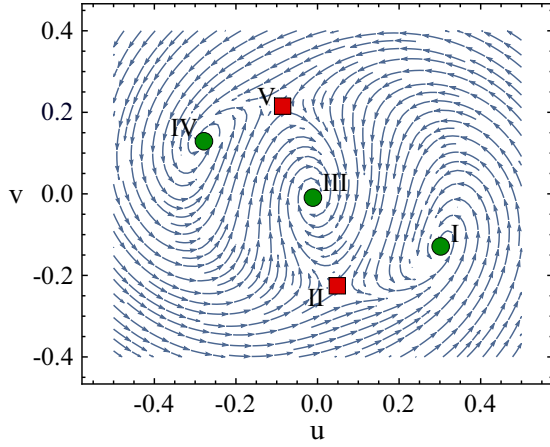
FIG. 1. Trajectories of the nonlinear parametric resonator in slow variables u and v, obtained by numerically integrating Eqs. (7) and (8). The parameters chosen correspond to the unstable regime of the unforced linear parametric resonator: $\lambda = 5 \times 10^{-2}$, $\bar{F}_0 = 1 \times 10^{-3}$, $\bar{\gamma} = 1 \times 10^{-2}$, $\bar{\eta} = 3 \times 10^{-1}$, $\vartheta = 0$, and $\Omega = 1.03$. The green circles denote stable solutions, while red squares unstable ones.

requires a nonperturbative approach or the retention of higher-order corrections.

IV. RESULTS

A. Response

As will be shown below, the interplay among the periodic external force, parametric drive, and nonlinearities leads to two qualitative different behaviors for the response depending on the position in parameter space. The solutions to the fifth-order polynomial [Eq. (9)] can be stable or unstable. The stabilities can be directly inferred from the basins of attraction for this equation, plotted in Fig. 1. We find that typically one has three stable solutions (I, III, and IV) marked by green dots and two unstable solutions (II and V) denoted by the red squares.

For small amplitudes of the parametric drive λ pertaining to the stable regime [see inset in Fig. 2(a)], the response shown in Fig. 2(a) is dominated by the external force and resembles that of the Duffing oscillator [25]. Here the stable solutions I and IV become degenerate and the response has two stable branches (I and III) and one degenerate unstable branch (II). As λ increases and one crosses over to the unstable regime of the underlying linear oscillator [see inset in Fig. 2(b)], the degeneracies of both stable and unstable solutions are broken corresponding to the three stable attractors and two saddle points shown in Fig. 1. This generates a qualitatively different response as shown in Fig. 2(b), with an enhanced Duffing-type response encompassing an islandlike structure. This is due to a complex interplay among the cubic nonlinearity, the external force, and the parametric drive. We reiterate that this response cannot be obtained without the periodic external force. The splitting takes place even in the absence of noise-activated switching between the stable solutions, in contrast to previous studies [27].

As F_0 increases, the island is raised and shifted to larger frequencies. A sufficiently strong F_0 wipes out the internal island and the resulting frequency response is external force dominated and appears to be Duffing-like. In the limit $F_0 \to 0$,
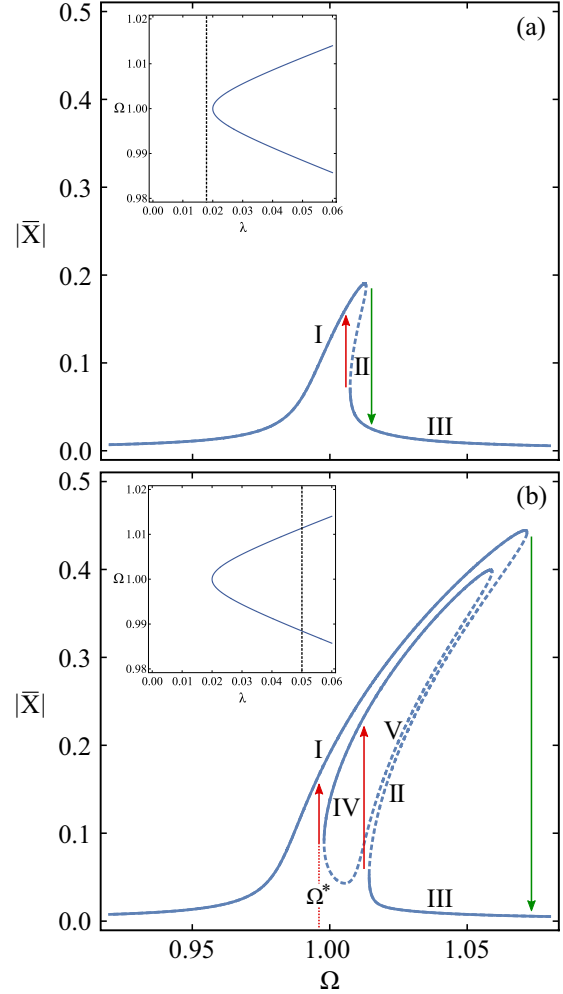

FIG. 2. Typical frequency responses of the system described by Eq. (1). The insets show the first instability region (Arnold tongue) of the unforced linear parametric resonator ($\alpha = \eta = F_0 = 0$) (continuous lines) and the chosen values of λ (dashed lines). (a) $\lambda = 1.8 \times 10^{-2}$ below the instability threshold (dashed line in inset); (b) $\lambda = 5 \times 10^{-2}$ above the instability threshold (dashed line in inset). Stable branches are indicated by whole lines, while unstable branches by dashed lines. The parameters $\bar{F}_0 = 1 \times 10^{-3}$, $\bar{\gamma} = 1 \times 10^{-2}$, $\bar{\eta} = 3 \times 10^{-1}$, and $\vartheta = 0$ are the same in both (a) and (b).

we recover the response shown in Appendix B, where I and IV (II and V) coalesce to a single stable (unstable) branch. The presence of F_0 thus leads to a splitting of the stable (unstable) branch into two stable (unstable) branches.

We now analyze the dependence of this novel response on the various tunable parameters in the system. The driving strength λ strongly affects both the maximal amplitude of the response as well as the frequency at which the intermediate stable branch originates. As λ increases, the intermediate branch dips further towards lower frequencies though the maximal response increases. Linear damping γ, on the other hand, simply shifts the stability boundaries of the linear parametric oscillator away from the $\lambda = 0$ axis [see inset in Fig. 2(a)]. As a result, for the response, it plays a role akin to the inverse of the driving strength λ, i.e., the larger the damping, the smaller the response

and the origin of the intermediate branch is pushed to higher frequencies. For sufficiently large damping γ, one enters the parameter region where the linear oscillator is stable and we recover the typical response of Fig. 2(a). Importantly, nonlinear damping η caps the response when ω increases, but it preserves the intermediate stable branch and the islandlike structure.

B. Force detection

We will now show that the amplitude of the near resonant periodic external force can be directly extracted from the qualitatively new response discussed earlier. The presence of stable and unstable branches in the response is expected to lead to hysteretic behavior during upward and downward sweeps of the frequency ω across ω_0. Consider the response for weak parametric driving plotted in Fig. 2(a). For upward sweeps of the frequency across ω_0, the response will gradually increase along branch I all the way to the maximal value where it hits the upper bifurcation and will then abruptly drop to the value of the lower stable branch III [green arrow pointing downwards in Fig. 2(a)]. For downward sweeps, the response slowly increases along branch III and then jumps abruptly to the stable branch I (red arrow pointing upwards). This is very similar to the standard Duffing-like hysteresis seen in many systems both in the presence and absence of an external force [1,25]. The sizes of the hysteretic jumps depend on many parameters, including F_0. It is highly nontrivial to extract the amplitude of the force from this hysteresis curve.

For λ in the unstable regime of the linear oscillator [cf. Fig. 2(b)], the presence of additional branches in the response leads to a new kind of hysteresis curve. For upward sweeps across the resonance frequency, the response will gradually increase all the way along branch I to the maximal value where it hits the upper bifurcation and will then abruptly drop to the value of the lower stable branch III. For downward sweeps, the response will increase very slowly across branch III until it hits the first bifurcation where it will abruptly jump to the stable branch IV of the island. It will then decrease further until it hits another bifurcation of the island at a frequency Ω^* where it will jump to the stable branch I. In short, the presence of stable solutions in the island results in two consecutive jumps in the downward sweeps.

The hysteretic jumps expected for the two response functions in the stable and unstable regimes are indicated in Fig. 2. Figure 2(b) shows a double jump hysteresis, whereas Fig. 2(a) shows the standard single jump hysteresis. The second jump in Fig. 2(b) is a direct manifestation of the intermediate stable branch discussed above and exists only when the amplitude of the external force F_0 is nonzero. The second jump is lost for high values of η as the island shifts to higher frequencies. This feature provides a promising new method to detect weak forces. The force F_0 can be extracted either from the magnitude of the second jump or from the frequency Ω^* at which it occurs.

We find that Ω^* depends linearly on F_0 for a wide range of forces, allowing for a new and simple force detection scheme (see Fig. 3). The slope of Ω^* versus $\bar{F}_0$ ($\Omega^* = \omega^*/\omega_0$) defines a dimensionless sensitivity $\bar{\kappa}$ which can be translated into physical units through the relation $\kappa = \frac{\bar{\kappa}}{\omega_0^2}\sqrt{\frac{|\alpha|}{m^3}}$. The jump frequency, and thus the sensitivity, also depend on the relative
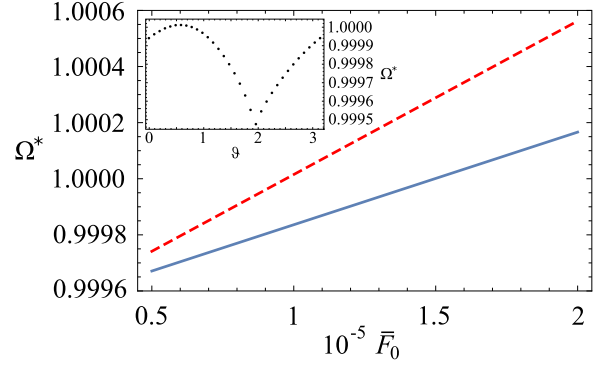

FIG. 3. Jump frequency Ω^* as a function of the strength of the external force for $\vartheta = \pi/4$ (red dashed line) and averaged over a uniformly distributed phase ϑ (blue solid line). The parameters are given by $\lambda = 0.016$, $\bar{\gamma} = 10^{-3}$, $\bar{\alpha} = 7 \times 10^{-3}$, $\bar{\eta} = 5 \times 10^{-3}$. The inset shows the phase dependence of the jump frequency Ω^* for a fixed value of the external force ($\bar{F}_0 = 1 \times 10^{-5}$).

phase between the periodic drive and the external force, as shown in the inset of Fig. 3. In the following, we consider the two cases that will be most relevant for experiments. On the one hand, if the phase ϑ of F_0 is stable and can be controlled, one can reach the maximum sensitivity κ_{max} that corresponds to $\vartheta \sim \pi/4$ (red dashed line in Fig. 3). On the other hand, if the phase of F_0 is fluctuating, then one effectively obtains a phase-averaged measurement with sensitivity κ_{mean} (blue solid line in Fig. 3). In Fig. 4, we plot the phase-averaged dimensionless sensitivity of the device ($\bar{\kappa}_{\mathrm{mean}}$) as a function of λ and $\bar{\eta}$. It is worth noting that as long as the parametric drive λ is beyond the instability threshold, the sensitivity *increases* with decreasing λ. We present values for both κ_{max} and κ_{mean} for typical experimental systems in the following section.

We note that a similar double jump hysteresis is expected for a system with negative Duffing parameter α where the response tilts towards the left (spring softening) [1]. In this case, Ω^* decreases linearly with increasing F_0 but the sensitivity, given by the magnitude of the slope, is expected to be the same as that for positive α. In other words, regardless of the sign of α, a direct
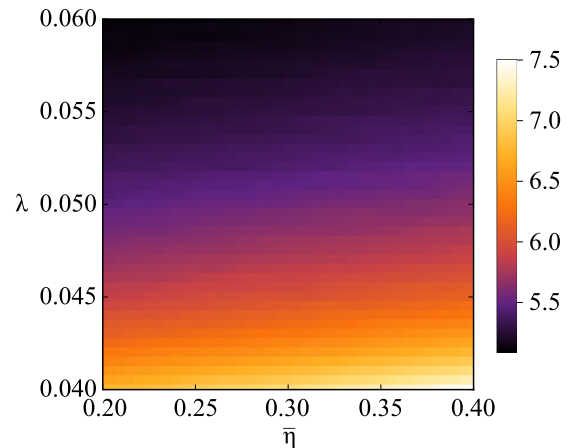

FIG. 4. Sensitivity $\bar{\kappa}$ as a function of the strength of the parametric drive λ and nonlinear damping $\bar{\eta}$. The force range $\bar{F}_0$ is from 5×10^{-4} to 1×10^{-3}, and $\bar{\gamma} = 10^{-2}$. The other parameters are kept fixed.

measurement of the hysteresis curve in the nonlinear regime of the parametrically driven resonator permits a straightforward extraction of the amplitude of the external force.

Importantly, from an experimental perspective, one needs a nonlinear oscillator with well-characterized Duffing nonlinearity and with tunable parametric modulation as well as nonlinear feedback cooling. The latter is particularly useful in generating a sizable second hysteretic jump. The device should first be calibrated, i.e., its sensitivity κ should be obtained via a series of measurements of Ω^* for different values of known force amplitudes F_0. Once the sensitivity is known, the device can be used to measure the amplitude of an unknown external force.

V. DISCUSSION

We now discuss the magnitudes of the forces that can be detected via the double hysteresis scheme. We consider an external force to be in principle detectable when the frequency shift of the second hysteresis is larger than the frequency noise present in the system, that is, if

$$\kappa F_0 \geqslant \sigma_f, \tag{10}$$

where κ is the sensitivity of the device in physical units of angular frequency per force and we use σ_f to denote the total (angular) frequency noise expected during a measurement. The minimum detectable force is then given by $F_{\min} = \sigma_f/\kappa$.

We present estimates for the range of forces which can be detected with two different resonators. We first consider a laser-trapped nanoparticle in high vacuum [28] with a very high quality factor and a negative Duffing coefficient α. This system allows for a wide manipulation of the system parameters with small thermal noise. The system parameters are $m \approx 3 \times 10^{-18}$ kg, $\omega_0 \approx 2\pi \times 1.25 \times 10^5$ s^{-1}, $Q \approx 10^8$ (controlled through the air pressure), and $|\alpha| \approx 1.8 \times 10^7$ kg m^{-2} s^{-2}. The nonlinear damping due to feedback cooling can be tuned in a range around $\eta \approx 14$ kg m^{-2} s^{-1} and the amplitude of the parametric drive we use is $\lambda = 10^{-4}$, which is well inside the available modulation range. Calculating $\bar{\kappa}$ from solutions of Eq. (9) and then transforming into physical units, we obtain $\kappa_{\text{mean}} = 4 \times 10^{19}$ Hz/N and $\kappa_{\max} = 5.6 \times 10^{19}$ Hz/N. For a sweep duration of typically a few seconds, the frequency noise can be expected to be in the range of 2π kHz in units of angular frequency [23], which gives a minimum detectable force of about 110 aN and 160 aN for $\kappa_{\max}$ and κ_{mean}, respectively. Please note that the frequency noise used here is largely dominated by laser intensity noise and could in principle be decreased substantially.

The lightest nanomechanical resonators available today are made of individual carbon nanotubes. These resonators have pronounced nonlinearities and can be driven parametrically with high modulation depth [29]. Typical parameters are [22] $m \approx 10^{-20}$ kg, $\omega_0 \approx 2\pi \times 5 \times 10^7$ s^{-1}, $Q \approx 10^3$, $\eta \approx 10^3$ kg m^{-2}s^{-1}, $|\alpha| \approx 4 \times 10^{11}$ kg m^{-2}s^{-2}, and $\lambda = 2.5 \times 10^{-3}$. With these parameters, we get $\kappa_{\text{mean}} = 4.5 \times 10^{20}$ Hz/N and $\kappa_{\max} = 7 \times 10^{20}$ Hz/N. From the linewidth of the frequency sweep in Fig. 4 of Ref. [22], we estimate an upper bound for the frequency noise of $2\pi \times 5$ kHz in units of angular frequency, which result in minimum detectable forces of 45 aN and 70 aN for $\kappa_{\max}$ and κ_{mean}, respectively. The quality factor

we use here is quite conservative. Values of up to $Q = 5 \times 10^6$ have been measured more recently [30]. The same study also demonstrated significantly reduced frequency noise. However, it is not clear how the device will behave when driven into the nonlinear regime.

We expect weak thermal fluctuations to broaden the response and modify the size of the hysteretic jumps but leave Ω^* effectively unchanged. As a result, thermal noise will not have any qualitative impact on our detection scheme for devices with very high Q factors. Generically, we expect the force to be detectable as long as the second jump is visible above the background noise. This should hold true as long as the system parameters as well as noise are such that one avoids activation of degenerate states or higher energy states. Note that the combination of driving, nonlinearities, and noise could lead to phenomena similar to stochastic resonance in the present context, but the study of these aspects is beyond the scope of the present work.

To conclude, we have presented a new paradigm for sensitive detection of forces using nonlinear parametric resonators. Though based on the nonlinear dynamics of the resonator, our measurement scheme is inherently linear. NEMS with relatively large Duffing nonlinearity α are good candidates for our force detection scheme. For state-of-the-art devices, our scheme might allow the detection of forces in the 10- to 100-aN range. Furthermore, the high sensitivities associated with our detection scheme can potentially be exploited in the context of techniques such as nano-MRI aiming at great spatial resolution [31,32].

APPENDIX A: LINEAR PARAMETRIC OSCILLATOR

The response of the linear parametric oscillator in the presence of a periodic external force has been analyzed in Ref. [9]. In Eq. (1) we set $\alpha = \eta = 0$. In this case, we obtain the stability diagram with Arnold tongues shown in Fig. 5.

For the first instability lobe, this response can easily be calculated from the slow flow equations [cf. Eqs. (7) and (8)] and has the form

$$|\bar{X}| = \frac{\sqrt{(\bar{\gamma}\Omega)^2 + \sigma^2 + \left(\frac{\lambda}{2}\right)^2 + \lambda(\sigma\cos 2\vartheta + \bar{\gamma}\Omega\sin 2\vartheta)}}{(\bar{\gamma}\Omega)^2 + \sigma^2 - \left(\frac{\lambda}{2}\right)^2}, \tag{A1}$$

where $\bar{\gamma} \equiv \gamma/m\omega_0$ and $\Omega \equiv \omega/\omega_0$. Here we have chosen $\omega_p = 2\omega$ and $\omega_f = \omega$ with $\omega \approx \omega_0$, and we introduced the detuning parameter $\sigma = 1 - \Omega^2$.

The typical response for different regimes are plotted in Fig. 6(a). Here we see that parametric driving enhances or reduces the response depending on the relative phase between direct and parametric drives. For instance, for $\vartheta = \pi/4$ (respectively, $\vartheta = 3\pi/4$) we have a remarkable increase
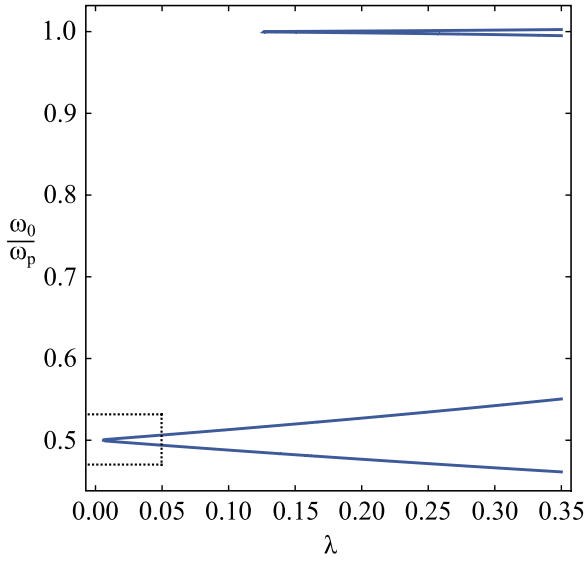
FIG. 5. First two instability regions (Arnold tongues) of the parametrically driven oscillator (continuous lines). The dashed box depicts the parameter region addressed in this work [cf. insets in Fig. 2].

(respectively, decrease) of the gain [see Fig. 6(b)]. Gain is here defined as $G = |\bar{X}|_{\lambda \neq 0} / |\bar{X}|_{\lambda = 0}$.
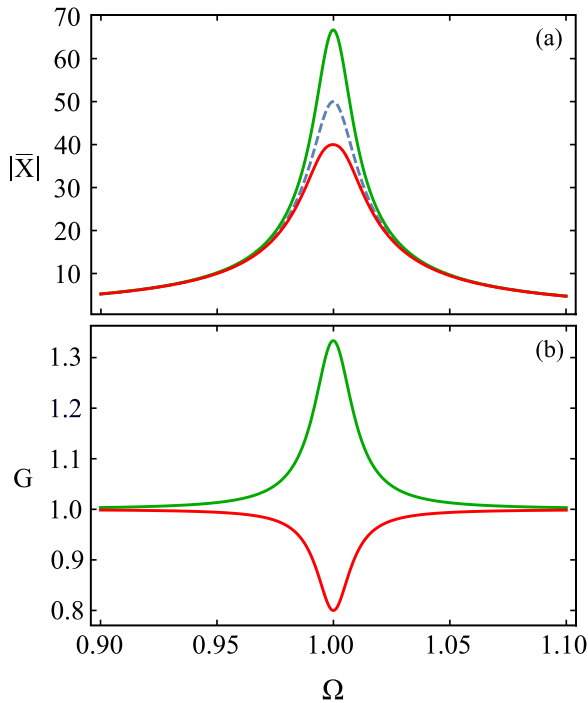

FIG. 6. (a) Typical frequency response for the usual harmonic oscillator (dashed line) and the parametric oscillator (continuous lines). For the red (lower) line $\vartheta = 3\pi/4$ the response is suppressed, while for the green (upper) line $\vartheta = \pi/4$ the response is enhanced. In (b) we show the gain for the same two phases.
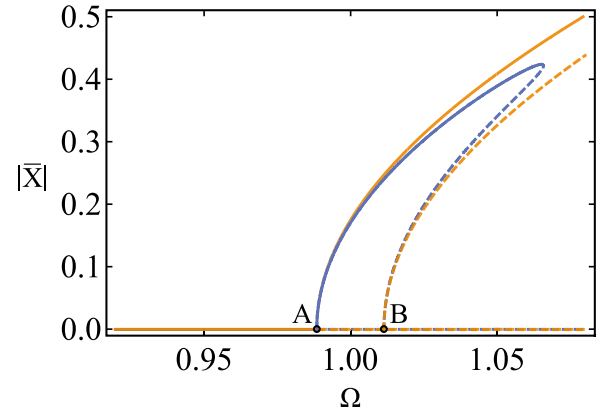

FIG. 7. Typical frequency response for an unforced nonlinear parametric oscillator with nonlinear damping $\eta \neq 0$ (blue) leading to a smaller response and without nonlinear damping $\eta = 0$ (orange) leading to a stronger response.

APPENDIX B: HOMOGENEOUS NONLINEAR PARAMETRIC OSCILLATOR

We now discuss the response of the nonlinear parametric oscillator in the absence of an external driving force. This will help clarify the effect of nonlinearities, both Duffing type as well as feedback cooling, on the shape of the response curves. In the absence of an external force $F_0 = 0$, the steady-state response has a trivial solution $|\bar{X}| = 0$ as well as nontrivial solutions satisfying the equation

$$\left(\bar{\gamma}\Omega + \frac{\bar{\eta}}{4}\Omega|\bar{X}|^2 \right)^2 - \left(\frac{\lambda}{2} \right)^2 + \left(\sigma + \frac{3}{4}|\bar{X}|^2 \right)^2 = 0. \quad \text{(B1)}$$

1. Zero feedback cooling ($\eta = 0$)

The nontrivial solutions for $\alpha \neq 0$ and $\eta = 0$ are given by

$$|\bar{X}|^2 = \frac{4}{3}\left(-\sigma \pm \sqrt{\left(\frac{\lambda}{2} \right)^2 - (\bar{\gamma}\Omega)^2} \right). \quad \text{(B2)}$$

The presence of the Duffing nonlinearity effectively stabilizes the parametric oscillator and allows us to explore the previous unstable region of parameter space. The oscillator displacement does not increase exponentially but saturates to a fixed amplitude. The frequency response of such a system (cf. Ref. [33]) is plotted in Fig. 7. It is characterized by three distinct regions with a different number of solutions each. In the first zone below A there is a single stable solution. The second zone between A and B has a high-amplitude stable solution and a zero-amplitude unstable one. The third zone beyond B has two stable solutions: a zero-amplitude and a high-amplitude one, as well as an unstable solution between the two stable branches. The extent of the second region, which is delimited by the occurrence of pitchfork bifurcations [21], is determined by the following equation $(\bar{\gamma}\Omega)^2 = (\lambda/2)^2 - \sigma^2$. This corresponds exactly to the equation for the first instability tongue [26]. The positive Duffing coefficient α results in a rightward tilt of the response, reflecting the effective hardening of the spring constant. Note that a negative Duffing term would result in a tilt towards the left, reflecting the softening of the

spring constant. This response has been measured in torsional Micro-electromechanical systems [34].

2. Feedback cooling ($\eta \neq 0$)

It is straightforward to assess the effect of nonlinear damping ($\eta \neq 0$) on the above response. The resulting response (cf. Ref. [24]), which is shown is Fig. 7, is qualitatively similar to the one obtained for $\eta = 0$. Nonlinear damping does not affect the bifurcations discussed earlier, but it principally limits the growth of the response as the frequency ω increases.

The detection of the width AB of the second region, which corresponds to tracing out the width of the Arnold tongue,

was proposed as a way to do high-precision mass sensing [19]. High precision is expected because of the sharp changes in the response amplitude at the boundaries of parametric resonance.

In both cases, the presence of stable and unstable solutions and a Duffing-like response is expected to lead to hysteretic behavior during upward and downward sweeps of the frequency ω across ω_0. For upward sweeps across the resonance frequency, the response will gradually increase all the way to the maximal value where it hits the upper bifurcation and will then abruptly drop to the value of the zero-amplitude stable branch. For downward sweeps, the response corresponds to the zero-amplitude stable branch until it hits the bifurcation point B, where it will abruptly jump to the outer stable branch of the response.

[1] A. H. Nayfeh and D. T. Mook, *Nonlinear Oscillations* (Wiley, New York, 2008).

[2] M. Dykman, *Fluctuating Nonlinear Oscillators* (Oxford University Press, Oxford, 2012).

[3] D. Rugar, R. Budakian, H. J. Mamin, and B. W. Chui, Nature **430**, 329 (2004).

[4] Y. T. Yang, C. Callegari, X. L. Feng, K. L. Ekinci, and M. L. Roukes, Nano Lett. **6**, 583 (2006).

[5] M. Poggio, Nat. Nano. **8**, 482 (2013).

[6] J. Chaste, A. Eichler, J. Moser, G. Ceballos, R. Rurali, and A. Bachtold, Nat. Nano. **7**, 301 (2012).

[7] M. Aspelmeyer, T. J. Kippenberg, and F. Marquardt, Rev. Mod. Phys. **86**, 1391 (2014).

[8] S. Aldana, C. Bruder, and A. Nunnenkamp, Phys. Rev. A **90**, 063810 (2014).

[9] D. Rugar and P. Grütter, Phys. Rev. Lett. **67**, 699 (1991).

[10] N. McLachlan, *Theory and Application of Mathieu Functions* (Clarendon, London, 1951).

[11] C. M. Caves, Phys. Rev. D **23**, 1693 (1981).

[12] M. A. Castellanos-Beltran and K. W. Lehnert, Appl. Phys. Lett. **91**, 083509 (2007).

[13] I. Mahboob, E. Flurin, K. Nishiguchi, A. Fujiwara, and H. Yamaguchi, Nat. Commun. **2**, 198 (2011).

[14] C. Eichler, Y. Salathe, J. Mlynek, S. Schmidt, and A. Wallraff, Phys. Rev. Lett. **113**, 110502 (2014).

[15] A. Szorkovszky, A. A. Clerk, A. C. Doherty, and W. P. Bowen, New J. Phys. **16**, 063043 (2014).

[16] I. Mahboob and H. Yamaguchi, Nat. Nano. **3**, 275 (2008).

[17] R. B. Karabalin, R. Lifshitz, M. C. Cross, M. H. Matheny, S. C. Masmanidis, and M. L. Roukes, Phys. Rev. Lett. **106**, 094102 (2011).

[18] H. W. C. Postma, I. Kozinsky, A. Husain, and M. L. Roukes, Appl. Phys. Lett. **86**, 223105 (2005).

[19] W. Zhang, R. Baskaran, and K. L. Turner, Sens. Actuat. A **102**, 139 (2002).

[20] L. G. Villanueva, E. Kenig, R. B. Karabalin, M. H. Matheny, R. Lifshitz, M. C. Cross, and M. L. Roukes, Phys. Rev. Lett. **110**, 177208 (2013).

[21] R. H. Rand, Lecture notes on nonlinear vibrations (2000), http://www.tam.cornell.edu/randdocs.

[22] A. Eichler, J. Moser, J. Chaste, M. Zdrojek, I. Wilson-Rae, and A. Bachtold, Nat. Nano. **6**, 339 (2011).

[23] J. Gieseler, B. Deutsch, R. Quidant, and L. Novotny, Phys. Rev. Lett. **109**, 103603 (2012).

[24] M. C. Lifshitz and R. Cross, *Nonlinear Dynamics of Nanomechanical and Micromechanical Resonators* (Wiley-VCH, New York, 2009), pp. 1–52.

[25] J. Guckenheimer and P. Holmes, *Nonlinear Oscillations, Dynamical Systems, and Bifurcations of Vector Fields* (Springer-Verlag, Berlin, 1990).

[26] A. A. Batista, J. Stat. Mech.: Theor. Exp. (2011) P02007.

[27] D. Ryvkine and M. I. Dykman, Phys. Rev. E **74**, 061118 (2006).

[28] J. Gieseler, M. Spasenović, L. Novotny, and R. Quidant, Phys. Rev. Lett. **112**, 103603 (2014).

[29] A. Eichler, J. Chaste, J. Moser, and A. Bachtold, Nano Lett. **11**, 2699 (2011).

[30] J. Moser, A. Eichler, J. Güttinger, M. I. Dykman, and A. Bachtold, Nat. Nano. **9**, 1007 (2014).

[31] J. A. Sidles, Appl. Phys. Lett. **58**, 2854 (1991).

[32] C. L. Degen, M. Poggio, H. J. Mamin, C. T. Rettner, and D. Rugar, Proc. Natl. Acad. Sci. **106**, 1313 (2009).

[33] L. Landau and E. Lifshitz, *Mechanics* (Butterworth-Heinemann, London, 1976).

[34] H. B. Chan and C. Stambaugh, Phys. Rev. Lett. **99**, 060601 (2007).